Hydrothermal Synthesis and Luminescent Properties of Uniform $CaSnO_3$?:?$Eu^{3?+?}$ Microcrystals with Controlled Morphology

Zuoling Fu, Wenhao Li, Shan Du, Hyun Kyoung Yang and Jung Hyun Jeong

J. Electrochem. Soc. 2009, Volume 156, Issue 10, Pages J308-J311.
doi: 10.1149/1.3190536

Journal of The Electrochemical Society, **156** (10) J308-J311 (2009)
0013-4651/2009/156(10)/J308/4/$25.00 © The Electrochemical Society

Hydrothermal Synthesis and Luminescent Properties of Uniform $CaSnO_3:Eu^{3+}$ Microcrystals with Controlled Morphology

Zuoling Fu,[a,z] Wenhao Li,[b] Shan Du,[a] Hyun Kyoung Yang,[c] and Jung Hyun Jeong[c]

[a]*Key Laboratory of Coherent Light, Atomic and Molecular Spectroscopy, College of Physics, Jilin University, Ministry of Education, Changchun 130023, China*
[b]*Changchun Institute of Optics, Fine Mechanics and Physics, Chinese Academy of Sciences, Changchun 130033, China*
[c]*Department of Physics, Pukyong National University, Busan 608-737, South Korea*

$CaSnO_3:Eu^{3+}$ microcrystals with controlled morphology were prepared by a hydrothermal method followed by further calcining treatment without any template or capping reagents. Reactant concentration and reaction time showed strong effects on the phase formation and morphology of the products. The prepared samples were systematically characterized by powder X-ray diffraction, field-emission scanning electron microscopy, photoluminescence (PL), and photoluminescent excitation spectra. The possible formation mechanism was proposed. Furthermore, PL characterization of $CaSnO_3:Eu^{3+}$ microcrystals was performed and discussed in detail.
 [DOI: 10.1149/1.3190536]

Manuscript submitted May 7, 2009; revised manuscript received July 7, 2009. Published August 7, 2009.

Nanometer-sized inorganic low dimensional systems exhibit a wide range of optical and electric properties[1] that greatly depend on the crystal shapes due to the association between surface atomic arrangement and material stabilities.[2] Nowadays, research interests have been expanded into controlling the shape of materials and understanding the correlations between the materials properties and their microstructure and morphology.[3-5] However, attempts to prepare inorganic materials with uniform shape and size in large quantities still remain a challenge.[6-11] Considerable strategies have been developed for the growth of inorganic materials with different morphologies, such as flowerlike,[12] star-shaped,[13] and doughnutlike morphology products from inorganic precursors.[14] A further investigation on the parameters that controlled crystal growth was necessary to extend the obtainable inorganic materials with uniform shapes and sizes.

Recently, considerable interest in the optical and electrical properties of doped nanoparticles has emerged. Alternative classes of these materials that exhibit unique optical properties are those based on oxide-doped rare-earth ions.[15,16] The perovskite-type alkaline-earth stannates ($MSnO_3$, M = Ca, Sr, and Ba) have been extensively studied during the past century, especially on their very interesting application for display phosphor matrix, ceramic materials, thermally stable capacitors in electronic industries, and gas sensor host.[17-19] SnO_4^{2-} anions are reported to be optically inert and could be a candidate as a host material.[20] At present, many efforts have been devoted to the synthesis of $CaSnO_3$ microcrystals with various shapes by different methods.[21,22] $CaSnO_3$ microcubes can be prepared by a hydrothermal method with the assistance of polyvinylpyrrolidone surfactant.[21] Eight-horn or cubic $CaSnO_3$ microcrystals can be obtained by a precipitation method by the addition of a desired amount of NaOH or HCl solution to the Na_2SnO_3 aqueous solution.[22] However, little attention has been paid to the luminescence properties of alkaline-earth stannate phosphors.[23-27] Most of the preparation processes employ high calcination temperatures (800–1600°C [28]) or the products usually consist of particles with irregular shapes and wide size distributions. The methods mentioned in the literature required high temperature, special conditions, or tedious procedures. Therefore, the development of a mild and more controllable method for creating such architectures is of general interest. Recently, environmentally friendly synthetic methodologies that include molten-salt synthesis, hydrothermal process, and template synthesis have gradually been implemented as viable techniques in the synthesis of a range of materials.[29] In particular, the hydrothermal method as a typical solution-based approach has been proven to be an effective and convenient process in preparing various inorganic materials with diverse controllable morphologies and architectures.[30] In this work, we report a facile hydrothermal route to synthesize uniform $CaSnO_3:Eu^{3+}$ microcrystals with controlled morphologies at low temperature without any template or capping reagents. The possible formation mechanism has been proposed. Furthermore, the relation photoluminescent property of $CaSnO_3:Eu^{3+}$ microcrystal morphology was also investigated.

Experimental

Preparation of $CaSnO_3:Eu^{3+}$ nanocrystals.— Materials.— Calcium chloride dihydrate ($CaCl_2 \cdot 2H_2O$), sodium stannate trihydrate ($Na_2SnO_3 \cdot 3H_2O$), and europium nitrate pentahydrate [$Eu(NO_3)_3 \cdot 5H_2O$] were obtained from Aldrich. All of the chemicals were used without further purification. For the hydrothermal treatment, we used 80 mL Teflon cups.

Synthesis.— Calcium chloride dihydrate ($CaCl_2 \cdot 2H_2O$) and europium nitrate pentahydrate [$Eu(NO_3)_3 \cdot 5H_2O$] were dissolved in 20 mL distilled water and the mixture was stirred for 1 h. Sodium stannate trihydrate ($Na_2SnO_3 \cdot 3H_2O$) with different molar ratios of Ca: Sn was dissolved in another 20 mL distilled water and also stirred for 1 h. Then $Na_2SnO_3 \cdot 3H_2O$ solution was added to the previous solution and stirred again for 2 h. Finally, the mixture was placed in a poly(tetrafluoroethylene) (PTFE) vessel, and the vessel was capped by a PTFE cover and was placed inside a stainless steel autoclave. The autoclave was sealed and kept at 180°C for different reaction times followed by cooling down to room temperature. The precipitates taken from the autoclave were dried at 50°C in air. The precursor powders were calcined at 800°C for 3 h. Finally, eight-horn $CaSnO_3:Eu^{3+}$ microcrystals were obtained. To investigate the intermediates and luminescent properties of the eight-horn $CaSnO_3:Eu^{3+}$, the synthesis was stopped at different stages during the synthesis process. In addition, the activator's content (Eu) was maintained at 3 mol % for all the prepared samples.

Characterization.— The structural characteristics of the product were measured from the X-ray diffraction (XRD) patterns using a Philips XPert/MPD diffraction system with Cu Kα (λ = 0.15405 nm) radiation. The morphology and the size of the obtained samples were observed with field-emission scanning electron microscopy (FESEM, JSM-6700F, JEOL). For the optical investigation, the photoluminescence and photoluminescence excitation (PLE) measurements were obtained at room temperature by using a luminescence spectrometer (Photon Technology International, time-resolved fluorescence meter) with a Xe lamp as an excitation source.

[z] E-mail: zlfu@jlu.edu.cn

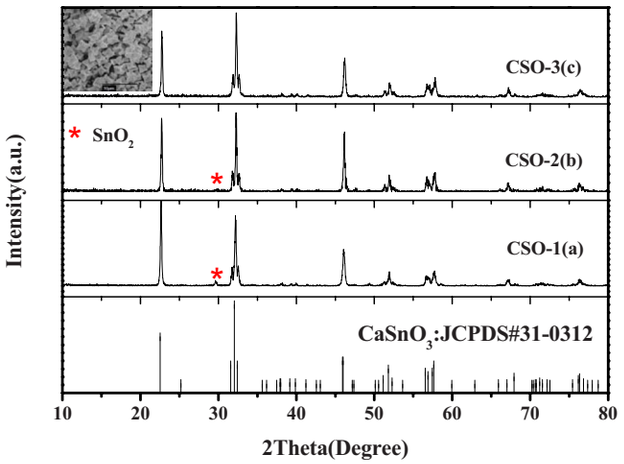

Figure 1. (Color online) XRD powder patterns of microcrystalline $CaSnO_3:Eu^{3+}$ with different molar ratios of Ca^{2+} to Sn^{4+}: (a) Ca:Sn = 1.1:1 (CSO-1), (b) Ca:Sn = 1.2:1 (CSO-2), and (c) Ca:Sn = 1.3:1 (CSO-3).

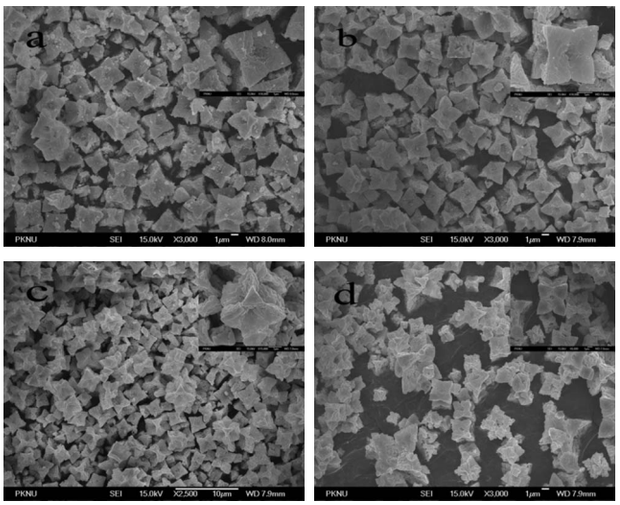

Figure 2. FESEM images of the products ($CaSnO_3:Eu^{3+}$ calcined at 800°C for 3 h) first synthesized at 180°C with different hydrothermal reaction times: (a) 2, (b) 4, (c) 7, and (d) 10 h.

Results and Discussion

Synthesis and morphology of $CaSnO_3:Eu^{3+}$.— Figure 1 shows the XRD patterns of the prepared $CaSnO_3:Eu^{3+}$ powders with different molar ratios. When the cations with the molar ratio of 1:1 (Ca:Sn) is calcined at 800°C for 3 h, the main phase is $CaSnO_3$; however, a few SnO_2 are formed (Fig. 1a, CSO-1). When the precursor powders with the molar ratio of 1.1:1 (Ca:Sn) are calcined at 800°C for 3 h, the diffraction peaks of SnO_2 became weaker (Fig. 1b, CSO-2). When the precursor powders with the molar ratio of 1.3:1 (Ca:Sn) are calcined at 800°C for 3 h, the SnO_2 disappeared completely, then the final product $CaSnO_3$ is formed (Fig. 1c, CSO-3). These XRD results reveal that the $CaSnO_3$ is crystallized to the pure orthorhombic phase with a 1.3:1 ratio of Ca:Sn after calcination at 800°C for 3 h. The XRD values of $CaSnO_3:Eu^{3+}$ samples roughly matched with $CaSnO_3$ standard values given in JCPDS card no. 31-0312. The lattice constants are calculated to be a = 5.808 Å, b = 5.540 Å, and c = 7.850 Å. It is suggested that the samples are of high crystallinity according to the intense diffractions. The FESEM image of sample (c) $CaSnO_3:Eu^{3+}$ microcrystals is shown in the inset (Fig. 1), which indicates that the microcrystal $CaSnO_3:Eu^{3+}$ synthesized by a hydrothermal method has an eight-horn shape.

To fully understand the effect of reaction time on the microstructure and morphology of the synthesized samples, controlled experiments were conducted to find the optimal morphology. Figure 2 shows the morphology of the products synthesized at 180°C with different hydrothermal times. At the early stages, we can get some eight-horn $CaSnO_3:Eu^{3+}$ microcrystals and part of the accumulated bulk crystals after a 2 h hydrothermal reaction (see Fig. 2a), and the surface of eight-horn $CaSnO_3:Eu^{3+}$ microcrystals is coarser, which distributed a small amount of single particle with the size of about 100 nm. When the reaction time was increased to 4 h (Fig. 2b), the product was mainly composed of eight-horn $CaSnO_3:Eu^{3+}$ microcrystals and a small amount of uncompleted eight-horn microcrystals. After 7 h of reaction, uniform, self-assembled, eight-horn microcrystals were finally synthesized, as shown in Fig. 2c. With a further increase in the reaction time to 10 h, part of the eight-horn microcrystals grew up and resulted in uneven morphology.

On the basis of the above discussion, our experimental results indicated that the molar ratio of the cations and the reaction time played an important role in the pure-phase formation and uniform morphology of eight-horn $CaSnO_3:Eu^{3+}$ microcrystals. A cation Ca:Sn ratio of 1.3:1 and a crystallization time of 7 h were optimal.

The formation mechanism for the eight-horn $CaSnO_3:Eu^{3+}$ microcrystals.— The crystal growth mechanisms in solution are so complicated that the actual crystallization mechanism remains an open question. Figure 3a and b shows the FESEM images of the $CaSn(OH)_6$ precursors before hydrothermal treatment with different precipitate times. At the early stages, Fig. 3a shows the coexistence of the four-horn-shaped microcrystal together with the single- or

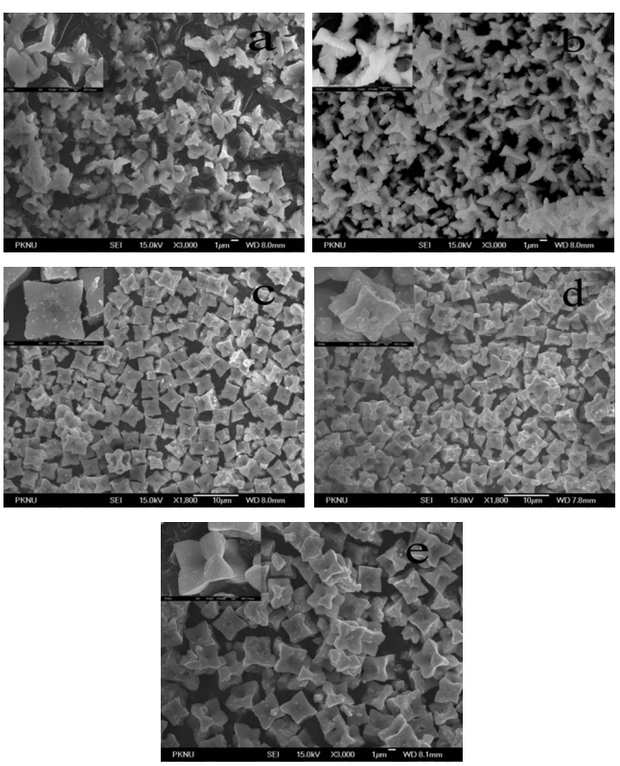

Figure 3. FESEM images of $CaSn(OH)_6$ before ahydrothermal reaction at room temperature with different reaction times [(a) 1 and (b) 7 h] and after a hydrothermal reaction at 180°C with different hydrothermal reaction times [(c) 2, (d) 4, and (e) 7 h].

double-horn crystals, which suggests that, eventually, the star-shaped crystals develop into eight-horn $CaSn(OH)_6$ microcrystals under hydrothermal conditions. Figure 3b shows the morphology of the products precipitated at room temperature for 7 h without hydrothermal reaction. It can be seen that the stars have eight symmetric arms of about 2 μm extending radially from the center. An arm shows a tridentlike, dendritic structure. At the middle stages of the hydrothermal reaction, the product was mainly composed of eight-horn $CaSn(OH)_6$ microcrystals and a small amount of uncompleted eight-horn microcrystals with the coarse surface (see Fig. 3c and d). If the products are synthesized after 7 h of hydrothermal treatment, it is visible that the as-synthesized eight-horn $CaSn(OH)_6$ microcrystals have a uniform size and an edge length of about 3 μm in the final stage of the reaction, as shown in Fig. 3e. In addition, it can be seen that there is a deep concave in the center of the eight-horn microcrystals.

It is concluded by Murphy[31] that the preferential absorption of molecules and ions in solution to different crystal faces directs the growth of nanoparticles into various shapes by controlling the growth rates along different crystal axes. Wang[32] suggested that the shape of a face-centered cubic crystal was mainly determined by the ratio of the growth rate in the ⟨100⟩ to that in the ⟨111⟩, and cubes bounded by the six {100} planes are formed when the ratio is relatively lower. Ma et al.[13] found that the faster growth on the {111} faces favors the formation of eight-arm PbS single crystals. The shape evolution of Cu_2O crystals ranging from eight-pod particles to star-shaped particles and then to cubes indicates that the formation of Cu_2O cubes in the study of Wang et al.[7] can also be attributed to the higher growth rate of {111} planes of the Cu_2O lattice. The views are verified by our experiments in the synthesis of eight-horn $CaSn(OH)_6$ microcrystals.

$CaSn(OH)_6$ crystallizes in the cubic structure, in which each Ca and Sn has six oxygen neighbors, respectively. For dendrites, a common explanation is that different growth rates of different surface sites finally result in branch growth. The {111} and {100} surfaces in the $CaSn(OH)_6$ crystal lattice are different in the surface atom structures and bonding as well as the possibility of chemical reactions. In the earlier stage of the reaction, once the $CaSn(OH)_6$ nuclei are formed, reactants continuously arrive at the site. The continuous growth on the different planes of $CaSn(OH)_6$ nuclei may kinetically favor the preferential crystal growth along eight ⟨111⟩ directions. As a result, the growth of $CaSn(OH)_6$ in the ⟨111⟩ direction leads to the formation of eight-pod particles (Fig. 3a and b). An increase in the temperature improves the reaction kinetics and results in an increase in reaction rates. In the following hydrothermal stage, the open spaces between the pods are gradually filled by the crystal growth of possibly the {110} and {100} planes, and in this way, the multipod particles gradually lost their shape (Fig. 3c and d). Eventually, the {111} facets were nearly eliminated because of their higher growth rate, and the {100} facets remained because they have the lower growth rate. An eight-pod microcrystal with six {100} planes is then obtained (Fig. 3e). The process of the morphology evolution of eight-pod $CaSn(OH)_6$ microcrystals is summarized in Scheme 1.

Luminescence properties.— Recently, considerable efforts have been devoted to research on phosphors used for white light-emitting diodes (w-LEDs) because w-LEDs have already begun to replace the traditional incandescent lamps and are expected to replace fluorescent lamps soon.[33,34] The proper red-emitting phosphor used for the near-ultraviolet (n-UV) LED should meet two primary requirements: (*i*) The phosphor host or the activator shows strong absorption in the n-UV spectral region and (*ii*) the phosphor could convert the n-UV light into red light efficiently. Eu^{3+} ion has been extensively investigated as an activator of the red-emitting phosphor due to its particular spectral character.[35,36] Figure 4 presents the room-temperature PLE spectra of $CaSnO_3:Eu^{3+}$ microcrystals. The PLE spectrum of $CaSnO_3:Eu^{3+}$ microcrystals exhibits a broad band between 200 and 350 nm, which is attributed to the charge-transfer transition between the Eu^{3+} ions and surrounding oxygen anions.[37] The sharp excitation lines are assigned to transitions between the $^7F_0$ and the $^5D_4$, ^5G_J, $^5L_6$, $^5D_3$, and $^5D_2$ levels at wavelengths of 362, 377, 383, 395, 417, and 466 nm. The strongest excitation line at 395 nm contributes to the $^7F_0 \rightarrow {}^5L_6$ transition in the n-UV region, which matches well with the commercial n-UV LED chip.

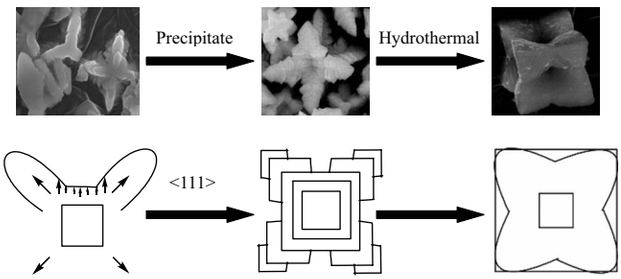

Scheme 1. Schematic illustration of the formation and morphology evolution of $CaSn(OH)_6$ microcrystals in the whole synthetic process.

Because the purpose of luminescent investigation is on the n-UV GaN-based LED phosphor, only the spectroscopic properties in the range of 350–400 nm were concerned. Therefore, only the emission spectra excited by 395 nm were shown in this paper. Upon UV excitation, the $CaSnO_3:Eu^{3+}$ phosphors exhibit a strong red luminescence. The emission spectra measured with the Xe lamp as an excitation source are shown in Fig. 5. The Eu^{3+} ion is sensitive to its surrounding environment, and the effect of the crystal field causes shifts and splittings of crystal-field levels. In $CaSnO_3:Eu^{3+}$, when Eu^{3+} ions replace the Ca^{2+} site (Ca occupies a C_s symmetry site with a noncentrosymmetric environment), the emission spectrum of $CaSnO_3:Eu^{3+}$ exhibits three obvious maxima located at 580, 592, and 614 nm, assigned to transitions from the excited $^5D_0$ state to ^7F_J (J = 0–2) levels of Eu^{3+}. For the $^5D_0$–$^7F_0$ transition, the initial and final energy states are nondegenerate, and only a single transition is expected (580 nm). It is also widely understood that the magnetic dipole transition $^5D_0$–$^7F_1$ is not dominant when Eu^{3+} ions in the crystal lattice occupy a site without an inversion symmetry. The $^5D_0$–$^7F_2$ transition is allowed when Eu^{3+} is embedded at a site of noninversion symmetry.[38,39] In this case, the emission peaks situated at 614 nm, showing a prominent and bright red light, are due to the

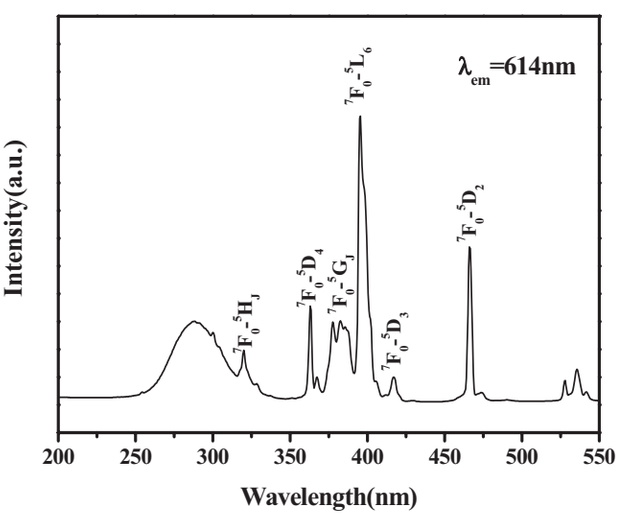

Figure 4. The excitation spectra of $CaSnO_3:Eu^{3+}$ microcrystals for the emission at 614 nm.

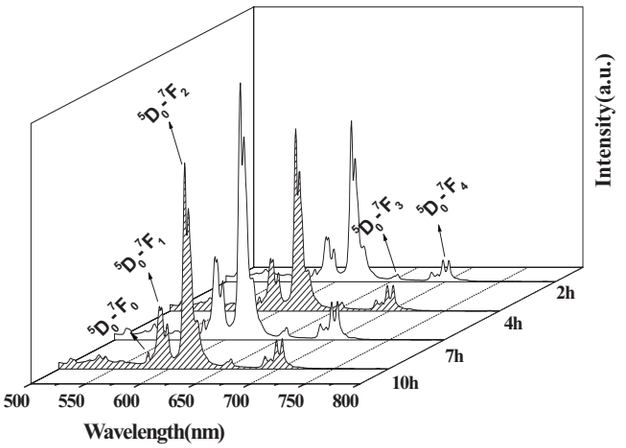

Figure 5. The emission spectra of $CaSnO_3$:Eu^{3+} prepared at different hydrothermal reaction times for the excitation at 395 nm.

$^5D_0$–$^7F_2$ electric dipole transition induced by the absence of inversion symmetry at the Eu^{3+} site, and it is much stronger than the orange $^5D_0$–$^7F_1$ transition (592 nm). Therefore, in the host material $CaSnO_3$ microcrystals, the emitting center does not occupy a site with a center of symmetry. In addition, comparing all the spectra in Fig. 5, it can be seen that the emission intensity with the best morphology (7 h) is the strongest. The excellent luminescence properties make it possible as a good candidate for LED application.

Conclusion

Eight-horn $CaSnO_3$:Eu^{3+} microcrystals have been successfully synthesized by a hydrothermal process followed by a further calcining treatment without any template or capping reagents. Suitable conditions for the synthesis of single-phase $CaSnO_3$:Eu^{3+} microcrystals were a cation Ca:Sn ratio of 1.3:1, a hydrothermal crystallization time of 7 h, and calcinations at 800°C for 3 h. The formation mechanism for the eight-horn microcrystals has been proposed on faster growth on the {111} faces. The emission peak situated at 614 nm, showing prominent and bright red light, is due to the $^5D_0$–$^7F_2$ electric dipole transition. The excellent luminescence properties make it possible as a good candidate for potential application in LEDs.

Acknowledgments

This work was supported by the Korea Research Foundation grant funded by the Korean government (MOEHRD, Basic Research Promotion Fund) (KRF-2007-412-J00902) and also partially supported by a grant-in-aid for the National Core Research Center Program from MEST and KOSEF (no. R15-2006-022-03001).

Jilin University assisted in meeting the publication costs of this article.

References

1. A. P. J. Alivisatos, *Science*, **271**, 933 (1996).
2. M. J. Siegfried and K. S. Choi, *Angew. Chem.*, **117**, 3282 (2005); M. J. Siegfried and K. S. Choi, *Angew. Chem., Int. Ed.*, **44**, 3218 (2005); R. E. B. Smalley and I. Yakobson, *Solid State Commun.*, **107**, 597 (1998); C. M. Lieber, *Solid State Commun.*, **107**, 607 (1998).
3. Z. Pan, Z. R. Dai, and Z. L. Wang, *Science*, **291**, 1947 (2001).
4. S. J. Bao, Q. L. Bao, C. M. Li, T. P. Chen, C. Q. Sun, Z. L. Dong, Y. Gan, and J. Zhang, *Small*, **3**, 1174 (2007); Q. L. Bao, S. J. Bao, C. M. Li, X. Qi, C. X. Pan, J. F. Zang, W. L. Wang, and D. Y. Tang, *Chem. Mater.*, **19**, 5965 (2007).
5. S. J. Bao, C. M. Li, J. F. Zang, X. Q. Cui, Y. Qiao, and J. Guo, *Adv. Funct. Mater.*, **18**, 591 (2008); Y. Qiao, S. J. Bao, C. M. Li, X. Q. Cui, Z. S. Lu, and J. Guo, *ACS Nano*, **2**, 113 (2008).
6. X. M. Sun and Y. D. Li, *Chem. Commun. (Cambridge)*, **2003**, 1768.
7. D. B. Wang, M. S. Mo, D. B. Yu, L. Q. Xu, F. Q. Li, and Y. T. Qian, *Cryst. Growth Des.*, **3**, 717 (2003).
8. Y. G. Sun and Y. N. Xia, *Science*, **298**, 2176 (2002).
9. Y. B. Zhao, Z. J. Zhang, and H. X. Dang, *J. Phys. Chem. B*, **107**, 7574 (2003).
10. F. Dumestre, B. Chaudret, C. Amiens, M. C. Fromen, M. J. Casanove, P. Renaud, and P. Zurcher, *Angew. Chem., Int. Ed.*, **41**, 4286 (2002).
11. S. M. Lee, S. N. Choi, and J. W. Cheon, *Adv. Mater. (Weinheim, Ger.)*, **15**, 441 (2003).
12. S. W. Liu, J. G. Yu, B. Cheng, and Q. J. Zhang, *Chem. Lett.*, **34**, 564 (2005).
13. Y. R. Ma, L. M. Qi, and H. M. Cheng, *Cryst. Growth Des.*, **4**, 351 (2004).
14. J. B. Liang, J. W. Liu, Q. Xie, S. Bai, W. C. Yu, and Y. T. Qian, *J. Phys. Chem. B*, **109**, 9463 (2005).
15. I. W. Lenggoro, B. Xia, H. Mizushima, K. Okuyama, and N. Kijima, *Mater. Lett.*, **50**, 92 (2001).
16. H. Meyssamy, K. Riwotzki, A. Kornowski, S. Naused, and M. Hasse, *Adv. Mater. (Weinheim, Ger.)*, **11**, 840 (1999).
17. A. M. Azad, M. Hashim, S. Baptist, A. Badri, and A. Ul. Haq, *J. Mater. Sci.*, **35**, 5475 (2000).
18. S. W. Tao, F. Gao, X. Q. Liu, and O. T. Sorensen, *Sens. Actuators B*, **71**, 223 (2000).
19. N. Sharma, K. M. Shaju, G. V. Subba Rao, and B. V. R. Chowdari, *Electrochem. Commun.*, **4**, 947 (2002).
20. S. Shionoya and W. M. Yen, *Phosphor Handbook*, CRC, Boca Raton, FL (1999).
21. H. Cheng and Z. G. Lu, *Solid State Sci.*, **10**, 1042 (2008).
22. C. H. Fan, X. Y. Song, H. Y. Yu, Z. L. Yin, H. Y. Xu, G. X. Cao, D. S. Zheng, and S. X. Sun, *Mater. Lett.*, **61**, 1588 (2007).
23. Z. W. Liu and Y. L. Liu, *Mater. Chem. Phys.*, **93**, 129 (2005).
24. Z. G. Lu, L. M. Chen, Y. G. Tang, and Y. D. Li, *J. Alloys Compd.*, **387**, L1 (2005).
25. B. F. Lei, B. Li, H. R. Zhang, and W. L. Li, *Opt. Mater. (Amsterdam, Neth.)*, **29**, 1491 (2007).
26. B. F. Lei, H. R. Zhang, L. M. Zhang, Y. Cong, and W. L. Li, *J. Electrochem. Soc.*, **154**, H623 (2007).
27. K. Goto, Y. Nakachi, and K. Ueda, *Thin Solid Films*, **516**, 5885 (2008).
28. A. M. Azad, L. L. W. Shyan, and P. T. Yen, *J. Alloys Compd.*, **282**, 109 (1999).
29. H. Zhou, Y. Mao, and S. S. Wong, *Chem. Mater.*, **19**, 5238 (2007); Y. B. Mao, T. J. Park, F. Zhang, H. J. Zhou, and S. S. Wong, *Small*, **3**, 1122 (2007).
30. L. Y. Wang and Y. D. Li, *Nano Lett.*, **6**, 1645 (2006); J. H. Liang, Q. Peng, X. Wang, X. Zheng, R. J. Wang, X. P. Qiu, C. W. Nan, and Y. D. Li, *Inorg. Chem.*, **44**, 9405 (2005); Y. Mao and S. S. Wong, *J. Am. Chem. Soc.*, **128**, 8217 (2006); R. Q. Song, A. W. Xu, and S. H. Yu, *J. Am. Chem. Soc.*, **129**, 4152 (2007).
31. C. J. Murphy, *Science*, **298**, 2139 (2002).
32. Z. L. Wang, *J. Phys. Chem. B*, **104**, 1153 (2000).
33. E. F. Schubert and J. K. Kim, *Science*, **308**, 1274 (2005).
34. Y. Q. Li, N. Hirosaki, R. J. Xie, T. Takeda, and M. Mitomo, *Chem. Mater.*, **20**, 6704 (2008).
35. L. H. Tian, B. Y. Yu, C. H. Pyun, H. L. Park, and S. Mho, *Solid State Commun.*, **129**, 43 (2004).
36. T. H. Kim and S. H. Kang, *J. Lumin.*, **122–123**, 964 (2007).
37. R. Schmechel, M. Kennedy, H. V. Seggern, H. Winkler, M. Kolbe, R. A. Fischer, X. M. Li, A. Benker, M. Winterer, and H. Hahn, *J. Appl. Phys.*, **89**, 1679 (2001).
38. B. R. Judd, *Phys. Rev.*, **127**, 750 (1962).
39. G. S. Ofelt, *J. Chem. Phys.*, **37**, 511 (1962).